Chinese Chemical Letters 32 (2021) 3076–3082

Contents lists available at ScienceDirect

Chinese Chemical Letters

journal homepage: www.elsevier.com/locate/cclet

Communication

Redox-responsive micelles integrating catalytic nanomedicine and selective chemotherapy for effective tumor treatment

Ronghua Jin[a,c], Zhongning Liu[b], Tao Liu[a], Pingyun Yuan[a], Yongkang Bai[a], Xin Chen[a,*]

[a] School of Chemical Engineering and Technology, Shaanxi Key Laboratory of Energy Chemical Process Intensification, Institute of Polymer Science in Chemical Engineering, Xi'an Jiao Tong University, Xi'an 710049, China
[b] Department of Prosthodontics, Peking University School and Hospital of Stomatology, National Engineering Laboratory for Digital and Material Technology of Stomatology, Beijing Key Laboratory of Digital Stomatology, Beijing 100081, China
[c] Pharmaceutical College, Guangxi Medical University, Nanning 530021, China

ARTICLE INFO

Article history:
Received 23 January 2021
Received in revised form 31 March 2021
Accepted 1 April 2021
Available online 2 April 2021

Keywords:
Chemotherapy
Gas therapy
Starvation therapy
Carrier-free
Tumor treatment

ABSTRACT

Chemotherapy is one of the most conventional modalities for cancer therapy. However, the high multidrug resistance of tumor cells still limited the clinical application of current chemotherapy. Considering the ability of nitric oxide (NO) to modulate potent P-glycoprotein to inhibit multi-drug resistance, a synergistic methodology combining chemotherapy and sustained NO generation is an ideal way to further promote the chemotherapy. Herein, a multi-functional micelle with tumor-selective chemotherapy driven by redox-triggered doxorubicin (DOX) release and drug resistance inhibition based on intracellular NO generation was fabricated for effective tumor treatment. The micelle consists of DOX as core, arginine/glucose oxidase (Arg/GOx) as shell and redox-responsive disulfide bond as a linker, which is denoted as micelle-DOX-Arg-GOx. The Arg serves as the biological precursor of nitric oxide for inhibition of multi-drug resistance to promote chemotherapy and GOx catalyzes glucose to produce hydrogen peroxide (H_2O_2) for increasing the generation of NO. Moreover, the glucose supply could be simultaneously blocked by the catalytic process, which further enhanced therapeutic efficiency. This micelle requests a tumor-specific microenvironment (a considerable amount of GSH) to perform synergistic therapeutics including chemotherapy, starvation therapy (catalytic medicine), and gas therapy for tumor treatment, which resulted in significant cytotoxicity to tumor tissue.

Malignant tumors, ranked as the leading cause of death in the world, pose a great challenge for human beings. While effective strategies for cancer therapy remain a challenge for physicians and clinicians. Among the existing theranostics, chemotherapy is one of the most conventional modalities for cancer therapy [1,2]. However conventional chemotherapy suffers from severe side effects and low efficiency due to the weak tumor selectivity of drugs and high multidrug resistance of tumor cells [3].

Nanocarriers with the ability to simultaneously achieve well-controlled intracellular drug release and meanwhile inhibit multidrug resistance to assist chemotherapy may be a solution to perform the efficacious tumor eradication [4–7]. Inspired by this idea, various nanocarriers such as liposomes [8], nanoparticles [9–13], drug polymer-conjugates [14,15] and micelles [16,17] have been developed, and various tumor-specific stimuli including redox, pH and enzyme were employed to trigger the intracellular drug release [18–21]. Among these drug carriers explored, micelles have been considered to be a promising candidate for controlled delivery of anticancer drug due to their unique advantages, such as their versatility to sundry therapeutic agents (hydrophobic compounds, metal complexes, and bio-macromolecules [22–24]), high drug loading capacity, on-demand drug release, high penetration to the deep tumor and ease tailoring of their surface.

Although a variety of nanocarriers have been synthesized for tumor treatment and shown well-controlled intracellular drug release triggered by tumor-specific microenvironment, the high multidrug resistance of tumor cells still limited the clinical application of current chemotherapy, resulting in relatively low therapeutic efficiency. To address this issue, strategies that combine chemotherapy with intracellular nitric oxide (NO) generation have been actively pursued to improve the therapeutic efficacy [25–27], due to the ability of NO to modulate potent P-glycoprotein to inhibit multi-drug resistance even at low concentration [28]. To perform specific stimuli-responsive NO

* Corresponding author.
E-mail address: chenx2015@xjtu.edu.cn (X. Chen).

https://doi.org/10.1016/j.cclet.2021.03.084
1001-8417/

release in tumor cells, considerable efforts have been devoted to developing biocompatible and activated NO donors including *N*-diazeniumdialates (NONOate) functionalized compounds and *S*-nitrosothiols (RSNO)-functionalized compounds [29–31]. However, the high toxicity of the by-product generated from NONOate and the rapid clearance of RSNO all limited their application *in vivo*. Recently, L-arginine (L-Arg) has been reported as NO donors because of its great biocompatibility and high efficiency for NO production [32,33]. However, the generation of NO from L-Arg depends on the concentration of H_2O_2 [34]. Disappointingly, the intracellular H_2O_2 concentration is relatively low even in tumor cells [35], which cannot provide a suitable environment to generate sufficient NO, severely limiting the therapeutic effect. Therefore, a synergistic methodology combining chemotherapy, L-Arg induced NO generation and simultaneous improvement of the intracellular H_2O_2 concentration during therapy is highly desirable.

Glucose, as an energy-yielding nutrient, can be burned as fuel to provide energy for tumor cell proliferation and metabolism. In view of the essential role of glucose in tumor cell multiplication, many researchers chose Glucose Oxidase (GOx) to catalyze glucose into gluconic acid and H_2O_2, the process of which can not only consume intracellular glucose for starvation therapy but also elevate intracellular H_2O_2 level to generate more NO for gas therapy. Therefore, the delivery of GOx to tumor cells is expected to deplete intra-tumoral glucose, blocking the energy supply and simultaneously increasing the H_2O_2 level for killing cancer cells, which leads to the emergence of a new paradigm of synergistic cancer-starving and oxidation therapy.

Herein, we designed and synthesized a redox-responsive micelle to perform on-demand synergistic chemo-gas therapy against solid tumor by L-Arg induced NO generation and GSH triggered DOX delivery in tumor cells. As to form the designed micelle, L-Arg and DOX were respectively used as hydrophilic and hydrophobic parts. Meanwhile, the PEG-modified cystamine was introduced as a redox-cleavable bridge to connect L-Arg and DOX for GSH triggered micelle deformation and subsequent drug release in tumor cells, due to the existence of disulfide bond in cystamine. To achieve efficient production of NO, GOx was co-delivered in the micelle, which is an enzymatic biocatalyst able to oxidize endogenous glucose into glucose acid and H_2O_2 [36]. The high glucose level inside tumor cells allows GOx to continuously generate H_2O_2 [35], which subsequently reacts with L-Arg to provide an environment rich of NO in tumor cells. These processes not only performed enhanced chemotherapy due to the synergistic effect of DOX and NO but also consumed the glucose in tumor cells, resulting in an additional starvation therapy (Scheme 1). We believe the micelle-DOX-Arg-GOx combining multiple model therapeutics would be a promising candidate for tumor therapy.

The design and synthetic process for the micelle-DOX-Arg-GOx are shown in Scheme 1. In order to endow the micelle with redox-responsiveness, we firstly conjugated cystamine with epoxide terminated PEG using the reaction between amino groups and epoxide groups to get the redox-cleavable bridge molecule with epoxide at both ends (EPO-PEG-ss-PEG-EPO). Then the epoxides at each side of EPO-PEG-ss-PEG-EPO were respectively reacted with DOX and Arg/GOx by controlling the ratio of the reactants, resulting in DOX-PEG-ss-PEG-Arg/GOx, which further assemble to form the final micelle-DOX-Arg-GOx. The stepwise synthesis of micelle-DOX-Arg-GOx was characterized by the Fourier transform infrared spectrum (Fig. 1a). As can be seen from these figures, characteristic vibrations of DOX, PEG, Arg, and GOx were all observed for the sample of micelle-DOX-Arg-GOx and DOX-PEG-ss-PEG-Arg/GOx. In details, the peak at 1285 cm^{-1} and 1621 cm^{-1} could be the bending vibrations of the amino group belonged to DOX, the shoulder peak at 1673 cm^{-1} belonged to the amino group of arginine, the peak located at 1082 cm^{-1} was attributed to the C—O stretching vibration of PEG, and the signal at 1648 cm^{-1} that should be attributable to the stretching vibration of amide bond of the GOx. All these results strongly indicated the successful fabrication of the micelle-DOX-Arg-GOx. To further confirm the successful conjugation of DOX and GOx, FITC labeled GOx was introduced into the micelle-DOX-Arg-GOx and then measured by fluorescence spectra. As shown in Fig. 1b, the micelle-DOX-Arg-GOx exhibited characteristic emission of DOX and FITC, indicating the existence of both GOx and DOX in micelle-DOX-Arg-GOx. Further information about the morphology of micelle-DOX-Arg-GOx was conducted by TEM, indicating a spherical

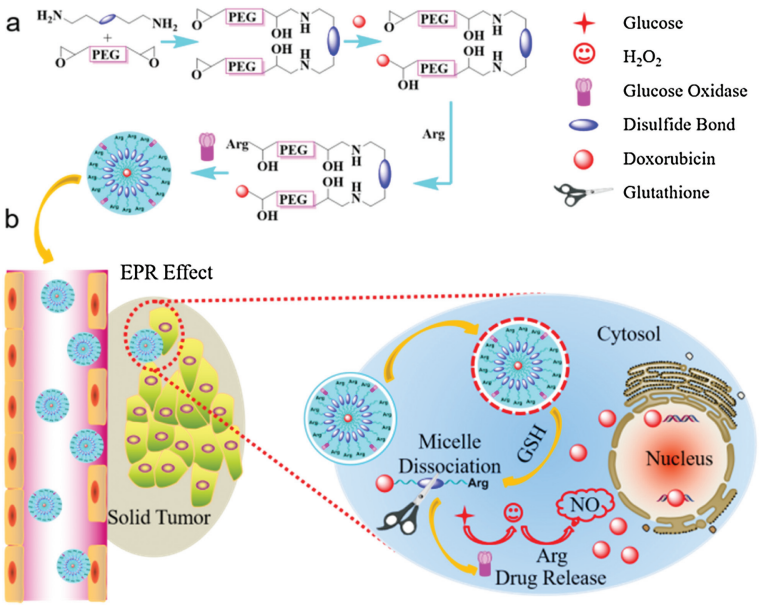

Scheme 1. Schematic illustration of the fabrication of micelle-DOX-Arg-GOx (a) and its actions for tumor therapy (b). The therapeutic mechanism of the micelles is initiated by GSH dependent cleavage of the disulfide bond, followed by DOX release to act on DNA in the nucleus (chemotherapy) as well as Arg/GOx triggered glucose consumption (starvation therapy) and NO production (gas therapy).

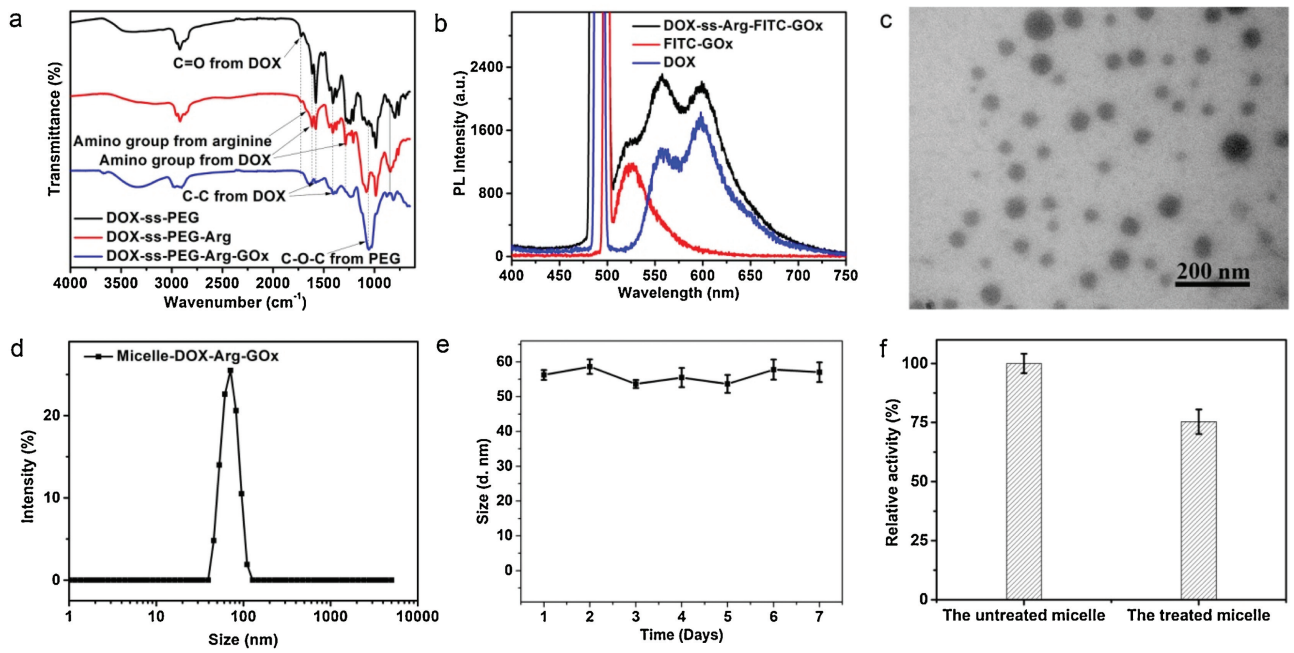

Fig. 1. (a) FTIR spectra of DOX-ss-PEG, DOX-ss-PEG-Arg, and DOX-ss-PEG-Arg-GOx to present the stepwise synthesis. (b) Fluorescence characterization of micelles formed by DOX-Arg-GOx containing FITC labeled GOx, free DOX and FITC labeled GOx. (c) Transmission electron microscope and corresponding particle size of micelles (insert) formed by DOX-Arg-GOx. (d) The size distribution of micelles formed by DOX-Arg-GOx (micelle-DOX-Arg-GOx) measured by dynamic light scattering. The average size was measured to be 56.06 nm. (e) The stability of micelle-DOX-Arg-GOx after 7 days incubation in PBS, which was determined by the hydrodynamic size changes of these micelles. (f) The relative activity of the micelle-DOX-Arg-GOx before and after 48 h PBS treatment.

structure with an average diameter of about 45 nm (Fig. 1c), which is in good accordance with the DLS result (Fig. 1d). Moreover, owing to the design of the self-delivery system, the micelle-DOX-Arg-GOx has a high loading capacity (25.3 wt%) of the therapeutic DOX.

As drug delivery systems for tumor therapy, continuously maintaining its structure and function in bio-system before arriving target place is also important. Thus, the size change and relative enzyme activity of micelle-DOX-Arg-GOx before and

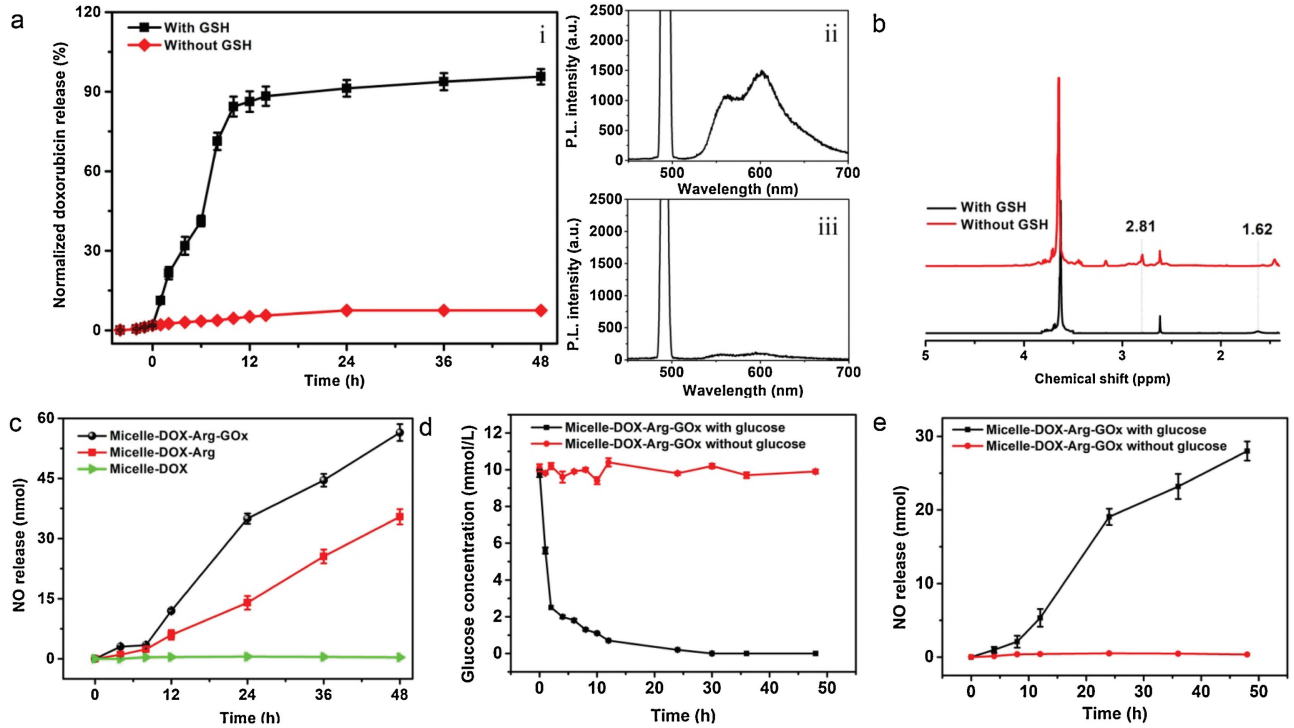

Fig. 2. (a) GSH-responsive release kinetics of micelle-DOX-Arg-GOx (i) and corresponding fluorescence spectrum of the leaching solution with/without GSH addition after 48 h incubation (ii, iii). Excitation wavelength: 490 nm. (b) ^{1}H NMR spectra of micelle-DOX-Arg-GOx before and after GSH treatment to demonstrate the mechanism of DOX release. (c) Accumulative generation kinetics of NO from different formulations with 10 mmol/L H_2O_2 and glucose (10 mmol/L) in PBS for 48 h. (d) Glucose (10 mmol/L) concentration change with and without addition of micelle-DOX-Arg-GOx, which was monitored by glucometer. (e) Accumulative generation kinetics of NO from micelle-DOX-Arg-GOx only with/without 10 mmol/L glucose in PBS for 48 h.

after incubation in a simulated physiological environment were investigated at first. As can be seen from Fig. 1e, the micelle-DOX-Arg-GOx always performed a constant size around 55 nm even after 7 days of incubation. Moreover, the micelles still maintain high activity even after 48 h incubation (Fig. 1f), which provide further evidence about the excellent stability of our micelle-DOX-Arg-GOx. The details of synthesis and characterization of micelle-DOX-Arg-GOx were presented in Supporting information.

Having confirmed the successful fabrication of micelle-DOX-Arg-GOx and its excellent stability, the stimuli-responsive release of DOX was investigated under simulated physiological conditions (PBS buffer with pH 7.4 in the presence/absence of GSH). The amount of DOX released from micelle-DOX-Arg-GOx was analyzed by monitoring the DOX emission spectrum at 600 nm as a function of time using fluorescence spectra. As can be seen from Fig. 2a, the final release amount of DOX in the absence of GSH is less than 3%. The negligible release could be attributed to the dissociation of a small amount of physically adsorbed DOX. In contrast, the release percentage of the DOX dramatically increased over time after GSH adding, which ends with the cumulative release of DOX up to 90% only in 24 h. This rapid DOX release could be ascribed to the disassembly of nanoparticles *via* cleavage of the disulfide bonds in a redox environment, which was verified by ^{1}H NMR. Fig. 2b showed complete disappear of resonances at δ 2.81 and new peaks appearance at δ 1.62, which could be attributable to the methylene protons neighboring to the disulfide bond (—CH_2—ss—CH_2—) and characteristic signal of thiol groups (—CH_2—SH), indicating that the DOX release was derived by GSH-triggered cleavage of disulfide bonds.

After the GSH-responsive release of DOX in tumor cells, the conjugated GOx would also dissociate from micelle, which was expected to convert tumorous glucose into H_2O_2. The resulting H_2O_2 could further react with the intracellular Arg delivered by micelle-DOX-Arg-GOx to generate NO, which would inhibit the P-glycoprotein (drug efflux transporter) to cut off DOX efflux [37], leading to increased tumor uptake of doxorubicin and enhanced chemotherapy. As to investigate these processes, the micelle-DOX-Arg-GOx induced NO generation in presence of glucose and H_2O_2 was quantitatively determined by a classical Griess assay. The micelle-DOX and micelle-DOX-Arg were used as control groups. As can be seen from Fig. 2c, negligible nitric oxide was observed for micelle-DOX even with H_2O_2. In contrast, both micelle-DOX-Arg and micelle-DOX-Arg-GOx exhibited obvious NO generation. However, micelles containing GOx performed 2-fold NO compared

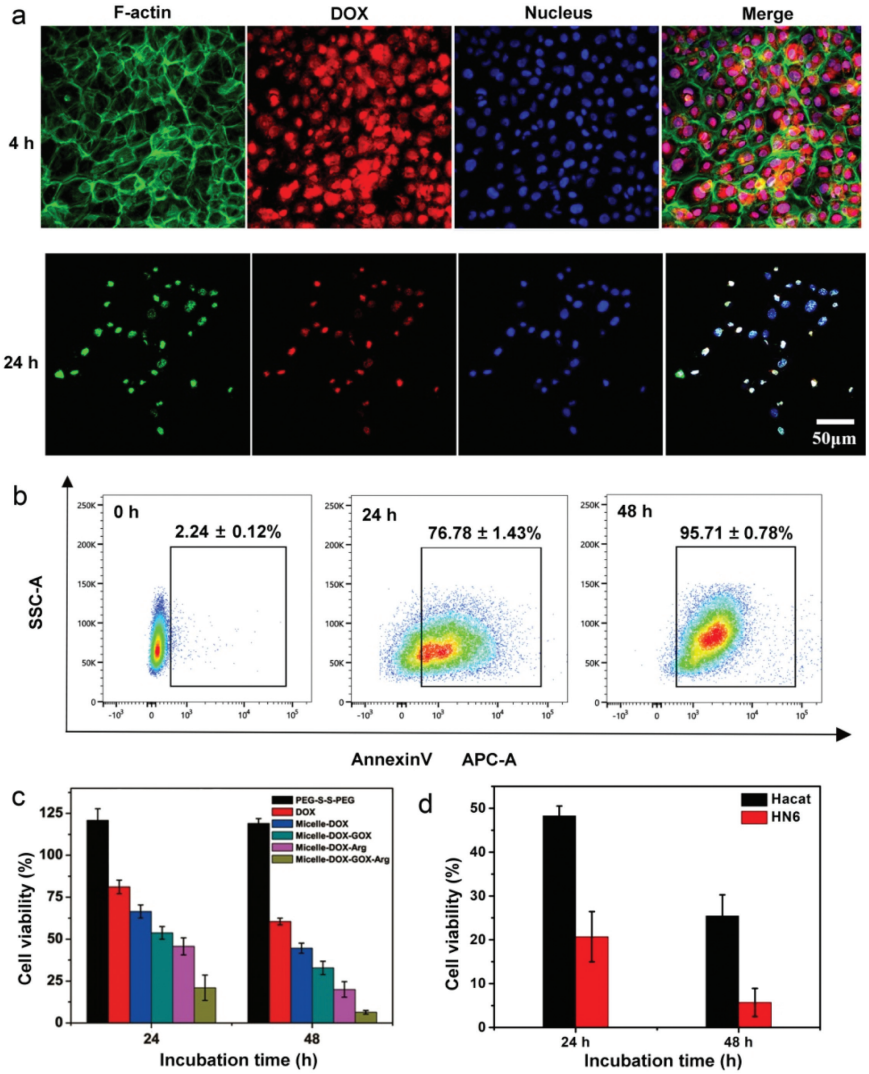

Fig. 3. (a) Confocal fluorescence microscopy images of WSU-HN6 cells at 4 h and 24 h after incubation with micelle-DOX-Arg-GOx. (b) FACS profiles of Annexin V-APC staining of WSU-HN6 cells undergoing apoptosis induced by micelle-DOX-Arg-GOx. (c) Cell viability of WSU-HN6 cells incubated with PEG-ss-PEG, pure DOX, micelle-DOX, micelle-DOX-GOx, micelle-DOX-Arg and micelle-DOX-GOx-Arg. (d) Cell viability of Hacat cells and HN6 cells after treatment with micelle-DOX-GOx-Arg for 24 h and 48 h, respectively.

with that of micelles without GOx, owing to the extra H_2O_2 production, which directly presented the activity of Arg and GOx in our micelles. More information was provided by the rapid glucose consumption and NO generation of micelle-DOX-Arg-GOx in PBS with glucose (Figs. 2d and e). All the results clearly indicate that the micelle-DOX-Arg-GOx could perform GSH triggered cascaded activities combining chemo-gas-starvation-therapy, which is an ideal candidate for cancer treatment. The details of measurement of NO release were presented in Supporting information.

As important factors to evaluate the therapeutic efficiency in cell level, the cellular endocytosis and intracellular drug release profiles of micelle-DOX-Arg-GOx were investigated using WSU-HN6 (a human oral squamous cell carcinoma cell line) by confocal laser scanning microscopy (CLSM). As showed in Fig. 3a, strong red fluorescence (DOX) was observed in the nucleus of WSU-HN6 cells only after 4 h incubation with micelle-DOX-Arg-GOx. The appearance of DOX in the cell nucleus is attributed to the property of free DOX as a DNA intercalating agent [38], which provides further information about the DOX release due to the mismatch of small nucleus pores and large micelle. Moreover, the cell numbers rapidly decreased meanwhile the cytoskeleton gradually destructed after increasing the incubation time to 24 h, which indicated the cytotoxicity of micelle-DOX-Arg-GOx to tumor cells.

Having demonstrated the uptake of micelle-DOX-Arg-GOx by tumor cells, Annexin V-APC staining was used to determine whether micelle-DOX-Arg-GOx can perform effective anti-tumor therapy. As shown in Fig. 3b, when WSU-HN6 cells were treated with micelle-DOX-Arg-GOx at 0 h, 24 h, and 48 h, the corresponding apoptosis rates were calculated to be 2.24% ± 0.12%, 76.78% ± 1.43%, and 94.68% ± 0.02%, respectively. The increasing percentage of apoptotic cells against the culture period indicated the great anti-tumor ability of our nanoparticles.

Having demonstrated the visual cytotoxicity of micelle-DOX-Arg-GOx, *in vitro* cytotoxicity of mono-therapy (pure DOX and

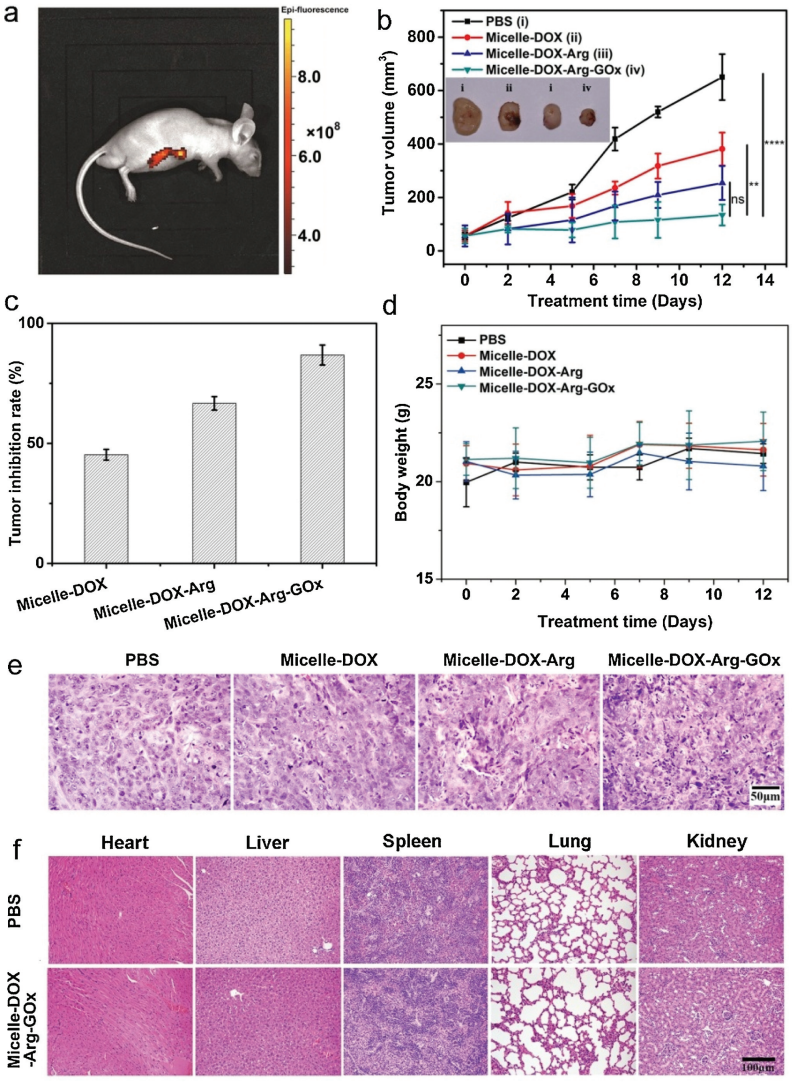

Fig. 4. (a) *In vivo* fluorescence images of the WSU-HN6 tumor-bearing mice after intravenous injection of micelle-DOX-Arg-GOx. (b) The WSU-HN6 tumor growth curve after intravenous injection of micelle-DOX (ii), micelle-DOX-Arg(iii) and micelle-DOX-Arg-GOx (iv) at a DOX dose of 2 mg/kg. The PBS (i) with equivalent volume was used as control. The insert shows digital images of tumor tissues collected from WSU-HN6 tumor-bearing mice after intravenous injection of PBS (i), micelle-DOX(ii), micelle-DOX-Arg (iii) and micelle-DOX-Arg-GOx (iv). Asterisks indicate P values associated with comparisons between the highest tumor inhibition rate and the other group; The significance of the results was analyzed by using one-way analysis of variance (ANOVA). $^{**}P < 0.01$; $^{***}P < 0.001$; ns, not significant. (c) The tumor inhibition rate after treatment with micelle-DOX, micelle-DOX-Arg and micelle-DOX-Arg-GOx. (d) Bodyweight variation after intravenous injection of PBS, micelle-DOX, micelle-DOX-Arg and micelle-DOX-Arg-GOx. (e) H&E image of tumor tissues collected from the WSU-HN6 tumor-bearing mice, which were sacrificed at 12 days after intravenous injection of PBS, micelle-DOX, micelle-DOX-Arg and micelle-DOX-Arg-GOx. (f) The histological analysis of main organs after 12 days treatment of PBS and micelle-GOX-Arg-GOx by HE staining.

micelle-DOX), dual-therapy (micelle-DOX-GOx and micelle-DOX-Arg), and triple-therapy (micelle-DOX-GOx-Arg) were tested to verify the synergistic superiority of our nanoparticles, which was measured by Cell Counting Kit 8 (CCK-8, Dojindo Co., Ltd., Japan) proliferation assay using WSU-HN6 and the same amount of DOX (0.5 μg/mL), while the incubation time is different. As can be seen from Fig. 3c, micelle-DOX showed certain cytotoxicity to tumor cells than pure DOX owing to the effective DOX delivery by our micelle. Relatively strong cytotoxicity was observed in the group of dual-therapy. However, the micelle-DOX-Arg exhibited stronger cytotoxicity than that of micelle-DOX-GOx, indicating the synergistic effect of chemo-gas-therapy is more efficient than that of chemo-starvation-therapy. As designed, the strongest cytotoxicity appeared in the group of micelle-DOX-Arg-GOx with triple-therapy, which performed only 7% surviving WSU-HN6 cells after 48 h incubation, indicating the all-in-one micelle-DOX-Arg-GOx can achieve an optimal antitumor effect. The tumor-selective cytotoxicity of micelle-DOX-Arg-GOx was also investigated by Cell Counting Kit 8 (CCK-8, Dojindo Co., Ltd., Japan) proliferation assay using both WSU-HN6 cells (tumor cells) and Hacat cells (normal cells). As can be seen from Fig. 3d, the micelle-DOX-Arg-GOx showed weak cytotoxicity to the Hacat cells with the viability of 48.27% and 25.45% for 24 h and 48 h. These viability values were 2-fold and 3-fold higher than that of HN6 cells (tumor cells) at the same concentration and incubation time, indicating high selectivity of our micelle for precise tumor therapy. All these results demonstrate that the micelle-DOX-Arg-GOx combined GSH–responsive chemotherapy, GOx/Arg triggered gas therapy and intracellular catalytic reaction-based starvation therapy would offer an effective anti-tumor property that could be potentially used to avoid the current challenge for cancer therapy. The details of *in vitro* experiments were presented in Supporting information.

The *in vitro* cytotoxicities firmly demonstrate that GSH-responsive micelle-DOX-Arg-GOx is promising for tumor therapy at the cell level. To verify the *in vivo* anti-tumor potential, the tumor-bearing mice were randomly divided into four groups and aliquots (100 μL) of aqueous solution of micelle-DOX-Arg-GOx (2 mg/mL) was intravenously injected into the tail vein. The bio-distribution of micelle-DOX-Arg-GOx was studied in WSU-HN6 tumor-bearing nude mice using an *in vivo* imaging system after 24 h post-injection. As shown in Fig. 4a, strong fluorescence (DOX) was mainly observed in the tumor, which reinforced the accumulation of micelle-DOX-Arg-GOx at the tumor site *via* the EPR effect. To further show the tumor therapy effect *in vivo*, tumor-bearing BALB/c mice were treated by different samples. The therapeutic efficacy was evaluated by monitoring the average tumor volume of different groups over a period of 12 days. As shown in Fig. 4b, the PBS treatment group showed almost no effect on tumor growth. However, the single chemotherapy group (micelle-DOX) and dual-therapy (micelle- DOX-Arg) showed different inhibition of tumor growth. The tumor inhibition rate of micelle-DOX and micelle-DOX-Arg were 45.3% and 66.7%, respectively (Fig. 4c). The combination group is more effective than the single group due to the synergistic effect. Particularly, in the triple therapy group combining chemotherapy, gas therapy, and GOx-based starvation therapy, the tumor inhibition rate reached up to 86.8%, indicating a great candidate for tumor therapy. The changes of body weight were further assessed to provide more evidence of the bio-safety of the micelles. As shown in Fig. 4d, the body weights of the mice had no notable changes during the treatment, which indicates the negligible side effects on the mice's health. To further evaluate the therapeutic efficacy, tumors in different groups were collected and histologically analyzed using hematoxylin and eosin (HE) staining (Fig. 4e). Compared with the control group (PBS group), tumors in the treatment groups showed different degrees of cell remission and apoptosis areas, among which tumors treated with micelle-DOX-Arg-GOx showed the largest area of cell degeneration with nucleolus broken up, confirming its high efficiency in suppressing tumor growth. Further evidence about the bio-safety of our micelle-DOX-Arg-GOx was provided by histological analysis of main organs from mice after treatment. As can be seen from Fig. 4f, all the main organs had no noticeable pathological abnormalities at the end of the treatment by micelle-DOX-Arg-GOx nanoformulation, which are similar to the PBS treated groups, exhibiting the excellent bio-safety of micelle-DOX-Arg-GOx. All the evidence strongly suggests that the micelle-DOX-Arg-GOx could serve as a platform for effective tumor treatment. The details of *in vivo* experiments were presented in Supporting information. All experimental protocols were approved by the Ethics Committee of the Peking University Health Science Center, Beijing, China.

In this study, we fabricated a novel micelle-DOX-Arg-GOx by conjugating DOX, Arg, and GOx with disulfide bonds as linkers to perform stimuli-responsive drug delivery and reverse the multi-drug resistance of tumor cells for effective tumor therapy. As design, the micelle-DOX-Arg-GOx is not only able to perform GSH triggered antitumor drug release but also simultaneously increase endogenous H_2O_2 to enhance NO production, which would reduce the drug resistance of tumor cells to further promote the chemotherapy. Moreover, this process also blocks the energy supply for starvation therapy, resulting in a great therapeutic effect. The *in vivo* data showed that tumors could be completely inhibited after 12 days of treatment with our synergistic method, which directly demonstrates the efficiency of our micelle for tumor therapy. This micelle is designed to not only integrate the advantages of chemotherapy, gas therapy, and starvation therapy but also take advantage of the unique physiological environment in tumor cells, making it an excellent candidate for therapeutic applications.

Declaration of competing interest

The authors declare that they have no known competing financial interests or personal relationships that could have appeared to influence the work reported in this paper.

Acknowledgments

This work was supported by the National Natural Science Foundation of China (No. 81601606to Xin Chen), the "Young Talent Support Plan" of Xi'an Jiaotong University (Xin Chen), the Technology Foundation for Selected Overseas Chinese Scholar of Shaanxi Province (Xin Chen), the Fundamental Research Funds for the Central Universities (No. 2016qngz02 to Xin Chen), the One Hundred Talents Program of Shaanxi Province (Xin Chen), National Natural Science Foundation of Shaanxi Province (No. 2017JM5023 to Xin Chen), open fund of the State Key Laboratory of Military Stomatology (No. 2017KA02 to Xin Chen), the Knowledge Innovation Program of Shenzhen (No. JCYJ20170816100941258 to Xin Chen), Beijing Nova Program of Science and Technology (No. Z191100001119096 to Zhongning Liu).

Appendix A. Supplementary data

Supplementary material related to this article can be found, in the online version, at doi:https://doi.org/10.1016/j.cclet.2021.03.084.

References

[1] X. Ding, F. Zhu, S. Gao, Food Chem. 131 (2012) 677–684.
[2] J. Zhou, G. Yu, F. Huang, Chem. Soc. Rev. 46 (2017) 7021–7053.
[3] J. Wen, K. Yang, F. Liu, et al., Chem. Soc. Rev. 46 (2017) 6024–6045.
[4] V.P. Torchilin, Nat. Rev. Drug Discov. 13 (2014) 813–827.

[5] R. Jin, J. Xie, X. Yang, et al., Biomater. Sci. 8 (2020) 1865–1874.
[6] Y. Lu, A.A. Aimetti, R. Langer, Z. Gu, Nat. Rev. Mater. 2 (2016) 16075.
[7] Y. Cui, R. Deng, X. Li, et al., Chin. Chem. Lett. 30 (2019) 2291–2294.
[8] L. Kong, Q. Chen, F. Campbell, et al., Adv. Healthc. Mater. 9 (2020) e1901489.
[9] R. Jin, Z. Liu, Y. Bai, et al., ACS Omega 3 (2018) 4306–4315.
[10] R. Jin, Z. Liu, Y. Bai, et al., Adv. Funct. Mater. 28 (2018) 1801961.
[11] R. Jin, Z. Liu, Y. Bai, et al., ACS Appl. Nano Mater. 1 (2018) 302–309.
[12] R. Cao, W. Sun, Z. Zhang, et al., Chin. Chem. Lett. 31 (2020) 3127–3130.
[13] A. Zhang, L. Hai, T. Wang, et al., Chin. Chem. Lett. 31 (2020) 3158–3162.
[14] L. Chen, Z. Liu, R. Jin, et al., J. Mater. Chem. B 6 (2018) 6262–6268.
[15] Y. Song, D. Li, J. He, et al., Chin. Chem. Lett. 30 (2019) 2027–2031.
[16] T. Liu, Z. Liu, J. Chen, et al., J. Biomed. Nanotechnol. 14 (2018) 1107–1116.
[17] J. Hu, Y. Xu, Y. Zhang, Chin. Chem. Lett. 30 (2019) 2039–2042.
[18] X. Jia, Y. Zhang, Y. Zou, et al., Adv. Mater. 30 (2018) e1704490.
[19] X. Hu, Z. Chai, L. Lu, et al., Adv. Funct. Mater. 29 (2019) 1807941.
[20] X. Chen, A.H. Soeriyadi, X. Lu, et al., Adv. Funct. Mater. 24 (2014) 6999–7006.
[21] R. Jin, Q. Wang, G. Dou, et al., Appl. Mater. Today 21 (2020) 100883.
[22] I. Gjuroski, E. Girousi, C. Meyer, et al., J. Control. Release 316 (2019) 150–167.
[23] Y. Dong, D.J. Siegwart, D.G. Anderson, Adv. Drug Deliv. Rev. 144 (2019) 133–147.
[24] F. Tosi, M.C.A. Stuart, S.J. Wezenberg, B.L. Feringa, Angew. Chem. Int. Ed. 58 (2019) 14935–14939.
[25] W. Fan, N. Lu, P. Huang, et al., Angew. Chem. Int. Ed. 56 (2017) 1229–1233.
[26] W. Fan, B.C. Yung, X. Chen, Angew. Chem. Int. Ed. 57 (2018) 8383–8394.
[27] M.F. Chung, H.Y. Liu, K.J. Lin, et al., Angew. Chem. Int. Ed. 54 (2015) 9890–9893.
[28] R. Guo, Y. Tian, Y. Wang, W. Yang, Adv. Funct. Mater. 27 (2017) 1606398.
[29] K. Zhang, H. Xu, X. Jia, et al., ACS Nano 10 (2016) 10816–10828.
[30] W. Fan, N. Lu, P. Huang, et al., Angew. Chem. Int. Ed. 56 (2017) 1229–1233.
[31] J. An, Y.G. Hu, C. Li, et al., Biomaterials 230 (2020) 119636.
[32] S. Kudo, Y. Nagasaki, J. Control. Release 217 (2015) 256–262.
[33] Z. Yuan, C. Lin, Y. He, et al., ACS Nano 14 (2020) 3546–3562.
[34] W. Fan, W. Bu, Z. Zhang, et al., Angew. Chem. Int. Ed. 54 (2015) 14026–14030.
[35] M. Huo, L. Wang, Y. Chen, J. Shi, Nat. Commun. 8 (2017) 357.
[36] W. Zhao, J. Hu, W. Gao, ACS Appl. Mater. Interfaces 9 (2017) 23528–23535.
[37] P.D.W. Eckford, F.J. Sharom, Chem. Rev. 109 (2009) 2989–3011.
[38] G. Minotti, P. Menna, E. Salvatorelli, et al., Pharmacol. Rev. 56 (2004) 185–229.